



Hydrogenation of CO₂ to methanol over CuCeTiO_x catalysts

Kuan Chang ^a, Tiefeng Wang ^{a,*}, Jingguang G. Chen ^{a,b,**}

^a Beijing Key Laboratory of Green Reaction Engineering and Technology, Department of Chemical Engineering, Tsinghua University, Beijing 100084, China

^b Department of Chemical Engineering, Columbia University, New York, NY 10027, United States

ARTICLE INFO

Article history:

Received 20 October 2016

Received in revised form 19 January 2017

Accepted 27 January 2017

Available online 30 January 2017

Keywords:

Cu catalyst

CeO₂–TiO₂

CO₂ hydrogenation

Methanol

ABSTRACT

Mixed oxides of CuCeO_x, CuTiO_x and CuCeTiO_x were prepared and evaluated for methanol synthesis via the hydrogenation of CO₂. A significant synergistic effect was observed between CeO₂ and TiO₂ as supports. The CuCeTiO_x catalyst was about 4 and 260 times more active than CuTiO_x and CuCeO_x, respectively, in terms of turnover frequency (TOF) values. The effect of changing the amounts of CeO₂, TiO₂ and CuO on the catalytic performance of CuCeO_x was also studied. With increasing content of CeO₂, the CO₂ conversion firstly increased and then decreased, with the CeO₂/TiO₂ weight ratio of 1 being optimal. An increase in the CuO content slightly enhanced the CO₂ conversion due to the increase of metal surface area. Kinetic experiments showed that the apparent activation barriers were lower for CO₂ activation and methanol synthesis over CuCeTiO_x than other Cu-based catalysts.

© 2017 Elsevier B.V. All rights reserved.

1. Introduction

The reduction of CO₂ emission has received significant attention because of climate change and ocean acidification related to the rising CO₂ concentrations in the atmosphere. The utilization of CO₂ by large-scale industrial conversion is more attractive among the various strategies to mitigate the CO₂ problem [1,2]. The direct hydrogenation of CO₂ to methanol has several advantages: (1) methanol is one of the top 10 petrochemicals, owning a worldwide annual production of 65 million tons [2–5]; (2) methanol is an important platform compound for the production of numerous chemicals, such as formaldehyde and acetic acid; (3) in addition to the C1 and C2 products, methanol can also be converted to olefins and aromatics (such as benzene, toluene and xylenes) through the methanol-to-olefins (MTO) and the methanol-to-aromatics (MTA) processes, respectively [1]; and (4) methanol can be directly added into gasoline, and can also be transformed to gasoline through the methanol-to-gasoline (MTG) process and to dimethylether (DME) as a diesel substitute by simple dehydration.

Among the methanol synthesis catalysts such as Cu-based catalysts, transition metal carbides (TMCs) [6–8], bimetallic catalysts

[5,9] and Au-based catalysts [10–12], Cu-based catalysts are the most widely studied and own many advantages. Apparently, Cu-based catalysts are lowest-cost compared with Au-based catalysts and bimetallic catalysts using Pd or Pt. TMCs catalysts such as Mo₂C produced CO or CH₄ rather than methanol. Although some TMCs such as TiC showed more catalytic activity than Cu surface for methanol production [7], the difficulty in the preparation of stable and high surface area TMC powder catalysts remained a challenge.

The most studied catalyst for methanol synthesis from CO₂ is CuO–ZnO–Al₂O₃ [13,14]. The main reactions related to this process include the hydrogenation of CO₂, hydrogenation of CO, water–gas shift reaction (WGSR) and reverse water–gas shift reaction (RWGS) [15]. Recent studies using DFT calculations and isotope tracer method suggest that the initial hydrogenation of CO₂ is an important step in controlling the activity and selectivity of methanol production [16–22]. These results point out the possibilities to improve methanol synthesis by promoting the adsorption and activation of CO₂ over the catalysts.

The reducible oxide supports, such as TiO₂ [14,17,18] and CeO₂ [16,19–23], have been found to be beneficial for both activity and selectivity in hydrogenation reactions. Although ZrO₂ [14,16,18,20–26] is not generally regarded as a reducible oxide, it often shows a similar capability to create oxygen vacancies as CeO₂ and TiO₂. The advantages of using this type of supports can be summarized to three aspects, namely enhancing the CO₂ adsorption, decreasing the CuO crystallite size and decreasing the H₂ dissociation temperature. Wang et al. [19] compared the CuO/Al₂O₃ catalyst with CuO/Al₂O₃–CeO₂ and CuO/Al₂O₃–Y-doped CeO₂ and observed that the presence of CeO₂ led to a significant enhancement in both

* Corresponding author at: Department of Chemical Engineering, Tsinghua University, Beijing 100084, China.

** Corresponding author at: Department of Chemical Engineering, Columbia University, New York, NY 10027, United States.

E-mail addresses: wangtf@tsinghua.edu.cn (T. Wang), jgchen@columbia.edu (J.G. Chen).

activity and selectivity. This enhancement could be ascribed to the synergistic effect of copper oxide and the surface oxygen vacancies of ceria by means of interfacial active centers. The methanol production activity and selectivity increase with increasing ceria loading and increasing yttria doping in ceria. Qi et al. [17] found that adding TiO_2 to the $\text{CuO}/\text{Al}_2\text{O}_3$ catalyst significantly decreased the CuO crystallite size and shifted the TPR peak toward lower temperatures.

The synergistic effect of mixed oxides has also been demonstrated. Xiao et al. [18] compared TiO_2 , ZrO_2 and $\text{TiO}_2\text{--ZrO}_2$ as supports for $\text{CuO}\text{--ZnO}$ catalysts and found that both TiO_2 and ZrO_2 decreased the crystallite sizes of CuO and ZnO and increased the surface area of metallic Cu. They also found that $\text{TiO}_2\text{--ZrO}_2$ mixed oxide supported $\text{CuO}\text{--ZnO}$ catalyst had enhanced amounts of basic sites and hydrogen adsorption.

The combination of TiO_2 and CeO_2 as catalyst supports has shown advantages in other catalysis applications. Maciel et al. [27] studied copper catalysts supported on CeO_2 and/or TiO_2 for WGSR. The addition of CeO_2 into the TiO_2 support hampered the transformation of anatase to rutile phase, and facilitated the reduction of metal species. As a result, the CuCeTi oxide catalyst showed a better activity than those using only CeO_2 or TiO_2 as support. Park et al. [28] studied the WGSR over $\text{M}/\text{CeO}_x/\text{TiO}_2$ ($\text{M} = \text{Au}, \text{Cu}, \text{and Pt}$) catalysts through a series of surface science experiments, and found that the $\text{M}/\text{CeO}_x/\text{TiO}_2(110)$ surfaces showed much higher catalytic activity for H_2 production than the $\text{M}/\text{TiO}_2(110)$ surfaces. At low coverages of Cu and CeO_x , $\text{Cu}/\text{CeO}_x/\text{TiO}_2(110)$ is 8–12 times more active than $\text{Cu}(111)$ or the Cu/ZnO industrial catalysts due to a strong synergistic effect between Cu and the mixed-metal oxide. The combination of CeO_2 and TiO_2 makes the CeO_x nanoparticles favor the +3 oxidation state [29].

The above studies suggest that $\text{Cu}/\text{TiO}_2\text{--CeO}_2$ may be active toward CO_2 conversion and can inhibit the RWGS in the hydrogenation of CO_2 compared with Cu catalysts supported on a single oxide. These favorable properties have also been predicted by Graciani et al. [30] through DFT calculations and surface science experiments. Similar studies were carried out on the $\text{Au}/\text{CeO}_2/\text{TiO}_2$ surface by Yang et al. [10], demonstrating that the $\text{CeO}_2/\text{TiO}_2$ interface could activate Au nanoparticles to more efficiently convert CO_2 molecules. In the present work, we report a novel Cu-based catalyst for methanol synthesis from CO_2 utilizing a strong synergistic effect between TiO_2 and CeO_2 , which presents excellent activity for methanol production compared with other Cu-based catalysts. The effects of chemical compositions and preparation methods were also studied to further improve the catalytic performance. The synergistic effect was discussed in detail with a combination of catalyst characterization and catalytic evaluation experiments.

2. Experimental

2.1. Catalysts preparation

The Cu catalysts supported on CeO_2 (CuCeO_x), TiO_2 (CuTiO_x) and $\text{CeO}_2\text{--TiO}_2$ (CuCeTiO_x) were prepared by the co-precipitation method. An aqueous solution of copper nitrate and/or cerium nitrate was prepared as the precursor. To avoid hydrolysis, the titanium tetrachloride precursor was added into cold water dropwise with a drip speed of 6 drops/min in an ice-water bath. The precursor was subsequently added into a 10 wt% soda solution dropwise while vigorously stirring under 343 K to achieve suspension. As demonstrated by Behrens et al. [31,32], the pH value for the precipitation of metal oxides played a vital role on the microstructure and thus catalytic performance of the final products. We optimized and controlled the $\text{CO}_3^{2+}/\text{M}$ ($\text{M} = \text{Cu} + 2\text{Ce} + 2\text{Ti}$, in mole) molar ratio as 1.2 in the precipitation. To eliminate the influence of Na^+ residue, the suspension was washed using deionized water, with a volume

ratio of water to suspension of 5 for five times. The sample was then dried at 363 K for 4 h. The dried samples were ground to fine powders and calcined for 4 h in air. Various calcination temperatures have been tested and 623 K was identified as the optimized temperature to produce best catalytic performance. The CuCeTiO_x catalysts with different compositions were prepared to study the effect of composition.

For the purpose of further studying the effects of preparation method and the catalysts compositions on the catalytic properties, the CuCeTiO_x catalysts were also prepared with the sol-gel (SG) method. Typically, 10 g $\text{Ti}(\text{OC}_4\text{H}_9)_4$, 3 mL CH_3COOH and 40 mL $\text{C}_2\text{H}_5\text{OH}$ were mixed under stirring to form solution A. The pH of solution A was adjusted to between 2.3 and 2.7 by HNO_3 . Solution B, consisting of required amounts of cerium nitrate and copper nitrate, 3 mL distilled water and 20 mL $\text{C}_2\text{H}_5\text{OH}$, was added dropwise to solution A under stirring until a stable sol was formed. The sol was aged to form gel and then dried at 343 K for 72 h. The dried samples were calcined under 723 K in air for 2 h.

2.2. Catalytic evaluation

The prepared catalysts were tested using a fixed-bed reactor. The gases, H_2 (99.995%) and CO_2 (99.995%), were used without further purification. The pressure of the reactor was controlled with a backpressure regulator. For each experiment, 1.2 g of catalyst was loaded in the reactor. Before reaction, the catalyst was reduced with a stream of 5% H_2/N_2 mixture by increasing the temperature to 573 K at a ramping rate of 1 K/min and holding at 573 K for 4 h. After the reduction, the temperature was decreased to 508 K and the system was pressurized to 3 MPa by feeding CO_2 at 10 mL/min and H_2 at 30 mL/min. The corresponding gas hourly space velocity (GHSV) was 2000 mL/(g-cat h). To obtain conversion-selectivity relationship, different GHSV values were employed by changing the gas flow and catalyst amount. In the kinetic experiments, the reaction temperatures varied from 463 K to 503 K.

The outlet stream was heated to avoid condensation and analyzed online by a gas chromatograph (GC, Techcomp, GC7980). Methanol and methane were analyzed with a flame ionization detector (FID), and CO and CO_2 were analyzed using a thermal conductivity detector (TCD).

2.3. Catalyst characterization

The powder X-ray diffraction (XRD) patterns were recorded on an automated powder X-ray diffractometer (40 kV, 40 mA, Bruker, Model D8Avance) using a $\text{Cu K}\alpha$ radiation source and a nickel filter in the 2θ range of 5–90° with step size of 2°/min. Raman spectra were obtained in the back-scattering configuration on a Laser Raman Spectrometer (LABRAM-HR800) using an Ar^+ laser (532 nm).

The surface area (SA) and pore volume (PV) were measured by low-temperature nitrogen adsorption/desorption (77 K, Autosorb-1-C, Quantachrome Co. Ltd) using standard BET and DFT methods, respectively. Before the adsorption measurements, the sample was degassed at 573 K under vacuum for 3 h. The catalyst morphology was characterized using a scanning electron microscopy (SEM, JEOL, JSM-7401F).

The capability of CO_2 adsorption was measured by CO_2 temperature programming desorption ($\text{CO}_2\text{-TPD}$) using a flow reactor equipped with a quadrupole mass spectrometry (QMS, Tilton Group Technology, LC-D200M PRO). For each measurement, about 50 mg of the catalyst was placed in a quartz tube reactor and outgassed at 523 K under He stream for 2 h. The sample was heated to 573 K at a ramping rate of 10 K/min in H_2 atmosphere and remained for 2 h. Then the reduced sample was purged with He for 15 min, and cooled to 300 K. After that, the sample was exposed to CO_2 for

20 min to adsorb CO₂ on the surface. This sample was then heated to 1023 K at a ramping rate of 10 K/min in He, during which the desorbed gases were subsequently detected by the MS and only the mass signal at *m/z* = 44 was recorded as the CO₂ desorption profile.

The surface and bulk compositions of the catalysts were measured with X-ray photoelectron spectroscopy (XPS) and inductive-coupled plasma-atomic emission spectrum (ICP-AES, Varian, Vista-MPX), respectively. The XPS measurements were performed on a high-performance electron spectrometer (ThermoFisher, 250XI) using Al-K α (1486.7 eV) radiation.

The dispersion and specific (chemically active) surface area of copper were determined by N₂O chemisorption using the same equipment of CO₂-TPD. For each measurement, about 100 mg of the catalyst was placed in a U-tube reactor and outgassed at 523 K under He for 1 h. After cooling to room temperature, the sample was heated to 573 K at a ramping rate of 2 K/min in 10% H₂/Ar mixture to completely reduce the copper. N₂O chemisorption experiments showed that CeTiO_x and CeO₂ had no reduction peaks below 573 K. Therefore, the CeTiO_x and CeO₂ did not contribute to the measurement of the Cu metal surface area. The amount of H₂ consumed was monitored by TCD and denoted as *n*₀. Then the reduced sample was cooled and exposed to a 10% N₂O/He mixture for 30 min to oxidize the surface copper. This sample was then reduced for the second time and the H₂ consumption was denoted as *n*_s. The dispersion of Cu (*D*_{Cu}) was calculated as:

$$D_{\text{Cu}} = \frac{2n_s}{n_0} \times 100\%$$

The specific surface area of copper (*S*_{Cu}) was calculated as:

$$S_{\text{Cu}} = \frac{w_{\text{Cu}} \times D_{\text{Cu}} \times N}{M_{\text{r,Cu}} \times 1.46 \times 10^{19}}$$

where *w*_{Cu} is the Cu mass fraction in the sample, *M*_{r,Cu} is the relative atomic mass of copper, *N* is the Avogadro constant, and 1.46 × 10¹⁹ is the number of copper atoms per square meter [33].

In order to achieve consistent sample pre-treatment, the samples for nitrogen adsorption/desorption, XPS and SEM characterizations were pretreated before the measurement. To do this, 200 mg of each sample was loaded in a quartz boat, which was then placed into a tube furnace. The sample was treated in 5%H₂/N₂ mixture in 573 K for 4 h with a heating rate of 1 K/min. After the furnace cooled down to room temperature, the samples were passivated by 1%O₂/N₂ mixture over-night.

3. Results and discussion

3.1. Synergetic effect of CuCeTiO_x catalysts

To investigate the synergetic effect of the CuCeTiO_x catalysts, the binary oxides, 30%CuO70%TiO₂ (CuTiO_x) and 30%CuO70%CeO₂ (CuCeO_x), and the ternary oxides 30%CuO35%CeO₂35%TiO₂ (CuCeTiO_x) were compared. The XRD patterns of the binary and ternary oxides are shown in Fig. 1. Ti oxide remained amorphous in the CuTiO_x and CuCeTiO_x catalysts. This result was different from those reported by Gao et al. [34] and Huang et al. [35], who observed an anatase phase in the CuCeTiO_x catalyst prepared by similar co-precipitation. The absence of crystallinity in the current samples was likely attributed to the short aging time and low calcinations temperature (623 K) used in the present work. In the CuCeO_x catalyst the CeO₂ peaks were well characterized, while in the CuCeTiO_x catalyst the CeO₂ peaks disappeared, suggesting the formation of a new phase consisting of the solid oxide solution of Ce and Ti. This phenomenon was consistent with previous studies of CeTiO_x oxides [36,37]. The reason is that Ti⁴⁺ (0.61 Å) is much smaller than Ce⁴⁺ (0.99 Å), therefore a higher Ti substitution should lead to the collapse of the CeO₂ cubic structure and the formation

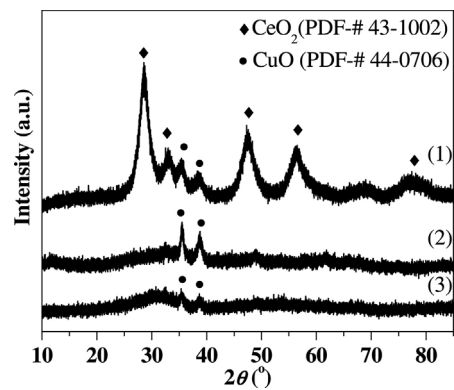


Fig. 1. XRD patterns of (1) CuCeO_x, (2) CuTiO_x and (3) CuCeTiO_x catalysts.

of a solid solution. In several previous studies, the formation of oxide solid solution of Ce and Ti has been proven vital for the catalytic properties, especially for reactions involving CO₂ [37,38], mainly because of the oxygen vacancy effect. Study regarding the reduction properties of Ce-Ti mixed oxides by Li et al. [38] demonstrated that Ti ions greatly weakened the Ce-O bond in CeTiO_x, making it easier to generate oxygen vacancies. Compared to CeO₂ and TiO₂, the mixed oxides of Ce and Ti were also characterized by a much higher H₂ consumption peak, consistent with the generation of more oxygen vacancies by H₂ reduction. Sheer et al. [39] also found that the incorporation of TiO₂ into the CeO₂ lattice could promote the reduction of both surface and bulk oxygen in the CeTiO_x supports for Pd/CeTiO_x catalysts. The solid oxide solution created defects throughout the crystal and led to an increase in the oxygen mobility and diffusion in the lattice. The experimental results were consisted with the DFT calculations, which predicted that the introduction of Th and Zr ions into CeThO_x [40] and CeZrO_x [41] solid solutions significantly decreased the energies required for the oxygen vacancy formation and migration. As shown in Fig. 1, the diffraction peaks of CuO were observed in all the three samples. However, in CuCeTiO_x the CuO peaks were much weaker, suggesting a higher CuO dispersion and smaller CuO crystallite on the CeTiO_x support. This result could be likely ascribed to the higher surface area of the ternary oxide supports, which will be discussed later.

The Raman spectra of CuCeO_x, CuTiO_x and CuCeTiO_x in Fig. 2 also suggest a molecular mixing of the oxides. In order to investigate the synergetic effect of the ternary oxide, TiO₂ and CeO₂ were prepared by the same co-precipitant method and characterized by Raman, then compared with commercial TiO₂ (rutile) and CeO₂ (cerianite) samples. The Raman spectrum of commercial TiO₂ showed three significant peaks at 235 cm⁻¹, 448 cm⁻¹ and 610 cm⁻¹, and the commercial CeO₂ sample showed one significant peak at 463 cm⁻¹. The synthesized TiO₂ and CeO₂ samples had similar peaks compared with the commercial samples. The slight differences of the Raman shift of each peak between the commercial and synthesized samples may be ascribed to either the presence of trace amount of residual Na⁺ or the difference in the oxide particle size. In comparison, the CuCeO_x, CuTiO_x and CuCeTiO_x samples showed different peak distributions, in particular CuCeTiO_x showed no obvious peaks in the region where the CeO₂ and TiO₂ peaks were expected, consistent with the formation of the oxide solid solution of Ce and Ti.

Another synergetic effect in the CuCeTiO_x ternary oxide is the significant increase of surface area compared with the CuCeO_x and CuTiO_x binary oxides. The surface area of CuCeTiO_x was 132 m²/g, which was about 5 times higher than that of CuCeO_x and 9 times higher than that of CuTiO_x. The pore volume data also showed substantial differences. The pore volume of CuCeTiO_x was 0.30 cc/g,

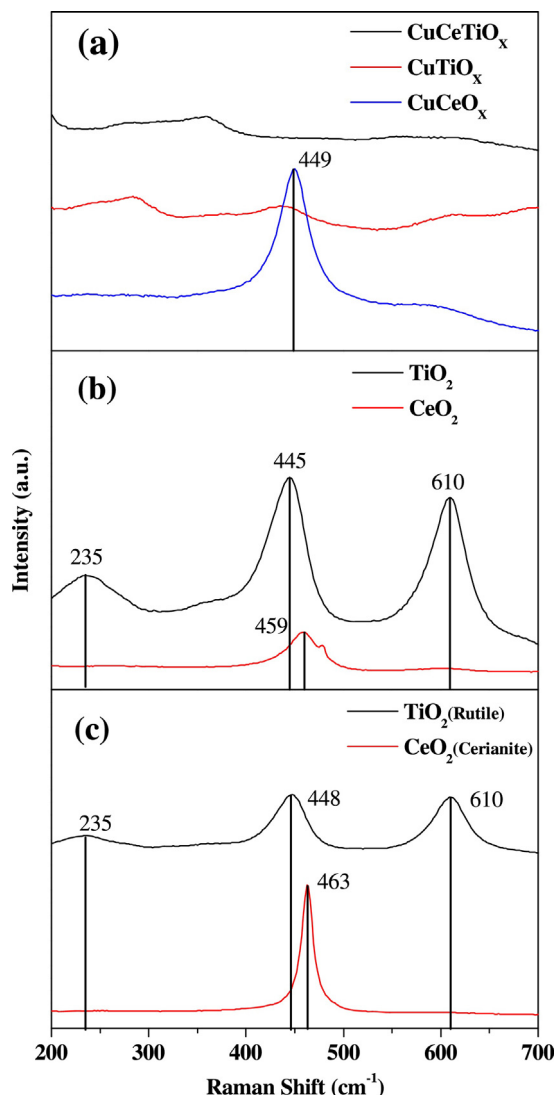


Fig. 2. Raman spectra of CuCeO_x, CuTiO_x and CuCeTiO_x catalysts (a), supports (b) and standard rutile, cerianite samples (c).

Table 1
Physical properties of CuCeO_x, CuTiO_x and CuCeTiO_x.

Catalysts	S.A. (m ² /g)	Pore volume (cm ³ /g)	D _{Cu} (%)	S _{Cu} (m ² Cu/g cat)
CuCeO _x	24	0.04	50.2	81
CuTiO _x	14	0.02	7.0	11
CuCeTiO _x	132	0.30	13.3	21

while those of CuCeO_x and CuTiO_x were 0.04 and 0.02 cc/g, respectively. These results are consistent with the SEM images, as shown in Fig. 3. The images in Fig. 3(a)–(c) showed that the CuCeO_x sample consists of flakes of about 20 μm in size and the CuTiO_x sample has a block-like morphology of similar size, while the CuCeTiO_x sample had a similar block-like morphology of much smaller particle size about 5 μm. Higher amplified pictures as illustrated in Fig. 3(d)–(f) show that CuCeTiO_x sample is uniquely characterized by a porous structure compared to the CuCeO_x and CuTiO_x samples.

The CuCeO_x, CuTiO_x and CuCeTiO_x catalysts were compared in the evaluation for the CO₂ hydrogenation reaction under 3 MPa at 508 K. The results of the physical properties are listed in Table 1. The Cu dispersion and metal surface area data obtained from N₂O chemisorption showed that the CuCeO_x sample had the largest metal surface area of 81 m²Cu/g cat, which was over 4 times higher than the other two samples. However, this catalyst gave the lowest methanol yield, indicating that not all the exposed Cu atoms are active for CO₂ hydrogenation to produce methanol.

The CuCeTiO_x ternary catalyst showed a much higher activity for the CO₂ conversion and methanol yield. Fig. 4 compares the product yields and TOF values (normalized by the surface area of Cu from N₂O chemisorption) for methanol synthesis over CuCeO_x, CuTiO_x and CuCeTiO_x. Both CuCeO_x and CuTiO_x showed very low activity for CO₂ conversion, while CuCeTiO_x demonstrated a much higher conversion of CO₂, approximately 7.4 and 12.0 times higher than that over CuCeO_x and CuTiO_x, respectively. Furthermore, the yield of methanol over CuCeTiO_x was much higher than that over both CuTiO_x and CuCeO_x.

Comparing these three catalysts in terms of TOF values, an even more significant synergistic effect is illustrated in Fig. 4(b). The TOF over CuCeTiO_x was about 4 and 260 times higher than that over CuTiO_x and CuCeO_x, respectively. The significant difference in the TOF values clearly indicates that the enhanced activity of CuCeTiO_x is from a synergistic effect, in addition to the difference in the surface areas of different catalysts. Such significant difference means that the active sites are not the same in these three

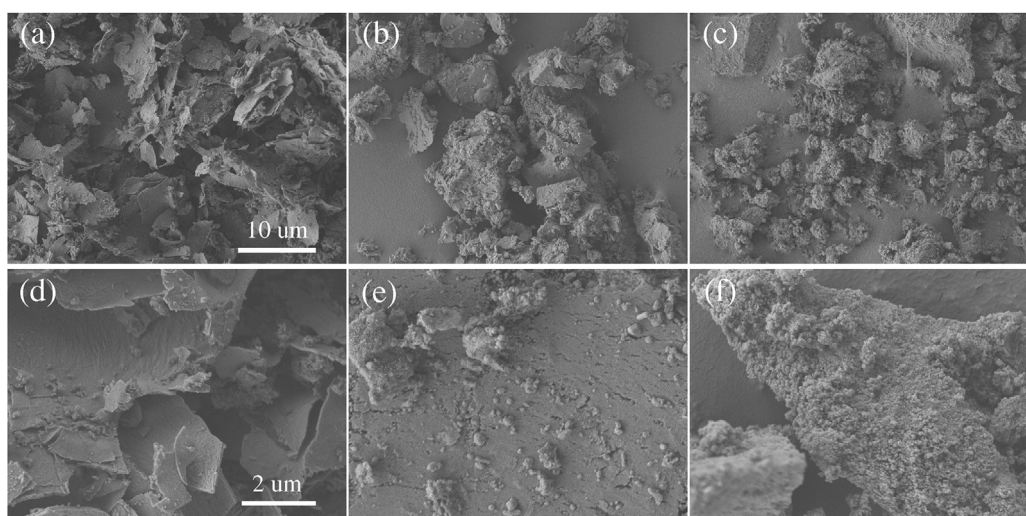


Fig. 3. SEM pictures of CuCeO_x (a, d), CuTiO_x (b, e) and CuCeTiO_x (c, f).

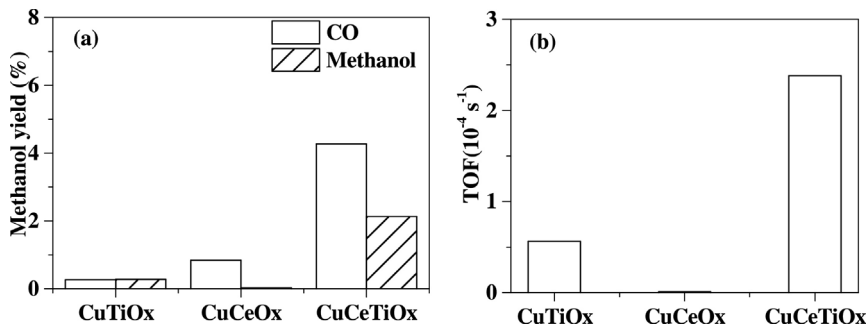
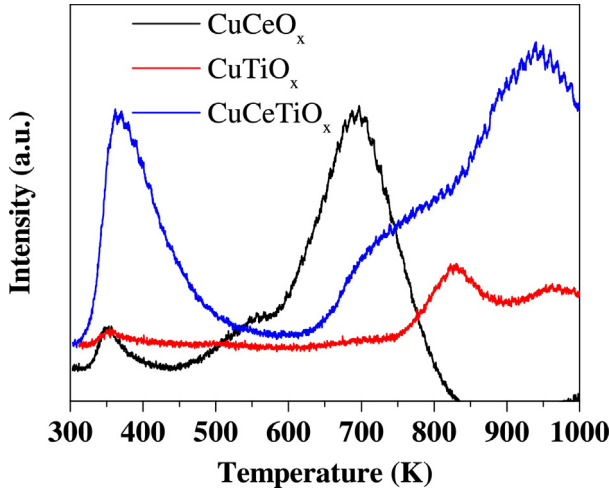
Fig. 4. Yield (a) and TOF for methanol (b) over CuCeO_x, CuTiO_x and CuCeTiO_x.Fig. 5. CO₂-TPD curves of CuCeO_x, CuTiO_x and CuCeTiO_x.

Table 2
Catalytic activity comparison of different Cu-based catalysts.

Catalysts	Methanol yield ($\mu\text{mol}/(\text{s g cat})$)	T (K)	P (MPa)	H ₂ /CO ₂ ratio	Ref.
CuCeTiO _x	0.13	508	3	3:1	This work
CuZnO/Al ₂ O ₃	0.60	503	3	3:1	[24]
Cu/SiO ₂	0.08	508	3	3:1	This work
Cu/Al ₂ O ₃	0.10	505	3	3.8:1	[45]
Cu/ZrO ₂	0.17	513	8	3:1	[12]

catalysts, and that the active sites on the CuCeTiO_x surface are more efficient for methanol synthesis. Combining with the XRD and Raman results, this enhancement could be explained by the formation of oxygen vacancies created by the molecular mixing of Ti and Ce in CuCeTiO_x. This is consistent with previous reports that oxygen vacancies play a very important role in CO₂ adsorption and activation [42,43] as well as the Cu charge state [44]. This conclusion was further verified by the CO₂-TPD characterization. Fig. 5 illustrates the CO₂ desorption curves from 300 K to 1000 K by measuring the mass signal at $m/z = 44$ using a mass spectrometer. Only weak desorption peaks were observed between 300 and 500 K for CuCeO_x and CuTiO_x. In comparison, the CuCeTiO_x showed a significant CO₂ desorption peak around 350–500 K, with a peak area approximately 12 times higher than that CuCeO_x. At temperatures over 600 K, significant CO₂ desorption peaks appeared for all the three catalysts, and CuCeTiO_x had a larger peak area than the other two catalysts. Overall, the TPD results showed that CuCeTiO_x had a higher capability of CO₂ adsorption, especially at moderate temperature, which benefited the reduction of CO₂. Table 2 compares CuCeTiO_x catalyst with other Cu-based catalysts in CO₂ hydrogenation. The Cu/SiO₂ catalyst was prepared by an

Table 3
Physical properties of different CuCeTiO_x.

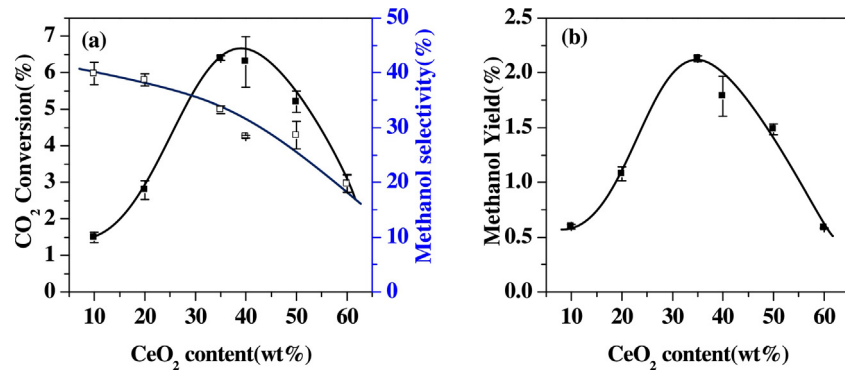
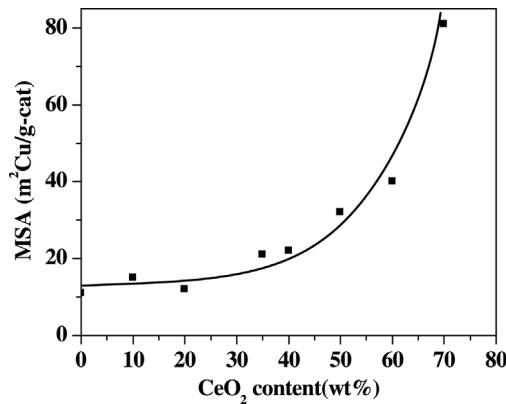
Catalysts	S.A. (m^2/g)	D _{Cu} (%)	S _{Cu} ($\text{m}^2/\text{g cat}$)
30Cu10Ce60Ti	161	9.0	15
30Cu20Ce50Ti	173	7.6	12
30Cu35Ce35Ti	132	13.3	21
30Cu40Ce30Ti	128	13.5	22
30Cu50Ce20Ti	107	19.8	32
30Cu60Ce10Ti	78	24.9	40
20Cu40Ce40Ti	149	11.6	13
40Cu30Ce30Ti	130	13.4	29

ammonia-evaporation method following Wang et al. [46]. Considering the addition of Zn could greatly change the Cu activity [47], Zn-free catalysts containing only Cu and oxides supports were compared. The comparison revealed that CuCeTiO_x had the highest methanol yield among all catalysts, except for Cu/ZrO₂. The slightly higher methanol yield on Cu/ZrO₂ was likely attributed to the much higher pressure. It should be pointed out that the catalytic performance of the CuTiO_x catalyst in the current work is different from some of the CuTi oxide catalysts reported in the literature [48,49]. In the current study the co-precipitation method was used to prepare the CuCeTiO_x mixed oxide catalysts, since it is a conventional method to obtain mixed oxide solid solution. In order to be self-consistent and to achieve a fair comparison, the CuCeO_x and CuTiO_x binary oxides were also prepared by co-precipitation. In comparison, the primary preparation method was impregnation for CuTi catalysts in the literatures, which are likely responsible for the observed difference in catalytic performance. Although not as competitive as the commercial CuZnAl-based catalysts, CuCeTiO_x has the potential to be further improved by introducing promoters, as has been done for improving the performance of the commercial catalysts.

3.2. Effect of composition in CuCeTiO_x

The effect of the elemental composition in the CuCeTiO_x catalyst on its physical properties and catalytic performance was further studied. Several CuCeTiO_x catalysts with different compositions were prepared, characterized and evaluated. As shown in Table 3, the surface area was greatly affected by the CeO₂ content. When the CeO₂ content increased from 10 wt% to 60 wt%, the surface area of CuCeTiO_x decreased from 161 to 78 m^2/g . Although the surface area of CuCeTiO_x changed greatly with the CeO₂ content, all these CuCeTiO_x catalysts had much higher surface areas than CuCeO_x or CuTiO_x. While a small amount of CeO₂ can prevent titania from sintering, the higher CeO₂ content can lead to surface area loss caused by the sintering of ceria itself. On the other hand, the presence of TiO₂ can inhibit the sintering of ceria, resulting in a higher surface area of the ternary oxides than the binary oxides.

Keeping the CuO content constant, the CO₂ conversion and methanol selectivity were affected by the CeO₂ content, as shown

Fig. 6. Effects of CeO₂ content on catalytic performance.Fig. 7. Effects of CeO₂ content on specific surface area of Cu.

in Fig. 6. With increasing content of CeO₂, the CO₂ conversion first increased, reached its maximum at a CeO₂:TiO₂ ratio of 1:1 (w/w), and then decreased with a further increase in the CeO₂ content. The methanol yield was 0.6% at CeO₂:TiO₂ = 1:6 (w/w), increased to 2.1% at CeO₂:TiO₂ = 1:1, and then decreased to 0.6% at CeO₂:TiO₂ = 6:1.

Fig. 7 shows the variation of the metal surface area (MSA), namely specific surface area of copper, as a function of the CeO₂ content. With increasing CeO₂ content, the dispersion and surface area of Cu remained almost unchanged at CeO₂ content below 40%, but increased significantly with a further increase in the CeO₂ content. At CeO₂ contents below 40 wt%, the increasing CeO₂ content improved the Cu dispersion but decreased the overall surface area of the catalysts. At CeO₂ contents above 40 wt%, the Cu dispersion was greatly enhanced, thus the Cu surface area increased despite the decrease in the overall surface area. However, the higher Cu dispersion did not lead to an increase in the CO₂ conversion or methanol yield, suggesting that the dispersion of Cu was not the

dominant factor for this reaction and that the oxide composition might play a more important role. This also suggested that not all exposed Cu atoms had the same activity for CO₂ conversion.

As shown in Fig. 8, when the CuO content increased at a constant Ce/Ti ratio, the conversion of CO₂ increased slowly and the selectivity to methanol remained almost unchanged. The increasing CO₂ conversion and methanol yield can be ascribed to the increasing amount of Cu active sites introduced by the higher CuO content, which was supported by the MSA data. The unchanged selectivity for methanol suggested that the catalytic property of Cu active sites did not change with the increasing CuO content.

3.3. Effect of preparation methods

Sol-gel is another conventional method to prepare mixed oxides, especially for M-CeTiO_x systems [50–52]. Burgos et al. [53] studied the mechanism of sol-gel transformation of Ti precursor and found that Ti alkoxides hydrolyzed at low pH formed the Ti-OH network. In the current study, it is assumed that Ce and Ti ions were hydrolyzed to form the framework at low pH during the sol-gel transformation and then the Cu ions were solidified with the evaporation of the solvents. Thus elemental distribution should differ between the bulk and surface, providing an opportunity to further study the effects of composition in CuCeTiO_x on their catalytic properties.

The 30%CuO35%CeO₂35%TiO₂ ternary oxide catalysts prepared by sol-gel (CuCeTiO_x-SG) and co-precipitation (CuCeTiO_x-CP) were compared. As shown in Fig. 9, the preparation methods had an important influence on the catalytic performance. The CuCeTiO_x-CP catalyst showed a higher CO₂ conversion than CuCeTiO_x-SG. However, the CuCeTiO_x-SG catalyst showed a higher selectivity to methanol than CuCeTiO_x-CP at the same CO₂ conversion. Additional studies, such as those performed for CO₂ conversion on supported Cu catalysts using DFT calculations and *in situ* IR measurements,

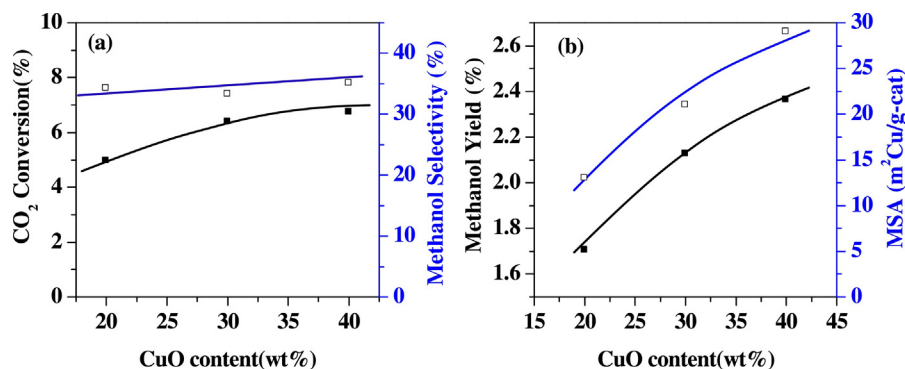


Fig. 8. Effects of CuO content on catalytic performance.

Table 4

Effect of preparation methods on catalyst physical properties.

Catalysts	S.A. (m^2/g)	S_{Cu} ($\text{m}^2\text{Cu/g-cat}$)	Compositions (CuO:CeO ₂ :TiO ₂ wt %)	
			Bulk	Surface
CuCeTiO _x -CP	132	21	30:30:40	31:32:37
CuCeTiO _x -SG	69	14	30:35:35	36:28:36

Table 5

Apparent activation energy for methanol synthesis over Cu base catalysts.

Catalysts	E_a -methanol (kcal/mol)	E_a -CO (kcal/mol)	Experiment pressure	Ref.
CuCeTiO _x	9	18	3 MPa	This work
Cu/CeO _x /TiO ₂ (1 1 0)	7	6	UHV	[30]
CeO _x /Cu(1 1 1)	12–13	11	UHV	[30,60]
Cu/ZnO(0 0 0 1)	16	14	UHV	[30]
Cu/ZnO(0 0 0 1)	16	14	0.5 MPa	[55]
Cu(1 1 1)	25	22	UHV	[30,60]
Cu(1 1 1)	25	22	0.5 MPa	[55]
Cu/ZnO	11	31	0.7 MPa	[63]
Cu/ZrO ₂	10	21	3 MPa	[62]
CuO-ZnO/ZrO ₂	14	30	1 MPa	[64]

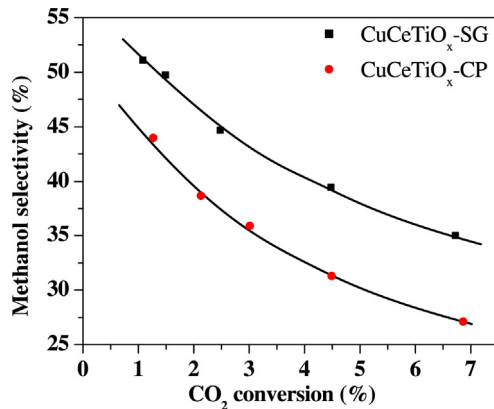


Fig. 9. Selectivity-conversion relationships of CuCeTiO_x-SG and CuCeTiO_x-CP.

[54] are necessary for a mechanistic understanding of changes in selectivity in Fig. 9.

Further characterization was carried out on these two samples and the results are listed in Table 4. The effect of preparation methods on the catalytic performance can be explained by the difference in surface composition. The XPS and ICP-AES results showed that although these two catalysts had similar bulk Cu composition, the surface Cu composition were quite different. The surface and bulk compositions were similar for CuCeTiO_x-CP, while for CuCeTiO_x-SG the surface Cu content was significantly higher than the bulk. The surface Cu content of CuCeTiO_x-SG was 36 wt%, much higher than that of CuCeTiO_x-CP. This result was consistent to the sol-gel formation mechanism discussed previously. The better selectivity for methanol over CuCeTiO_x-SG could be explained by its lower surface Ce/Ti ratio than that of CuCeTiO_x-CP, consistent with the effect of CeO_x/TiO_x shown in Fig. 6. The comparison also showed that CuCeTiO_x-CP had a much larger surface area than CuCeTiO_x-SG, because the drying of gel resulted in severe shrinkage and led to surface area loss [54]. These results explained why the CuCeTiO_x-SG showed a higher surface Cu content, but its Cu surface area was lower than CuCeTiO_x-CP.

3.4. Kinetic measurements

The reaction kinetics of CO₂ hydrogenation to methanol has been extensively studied, especially over Cu catalysts, in the form of either model surfaces or supported catalysts. The Cu(1 1 1)

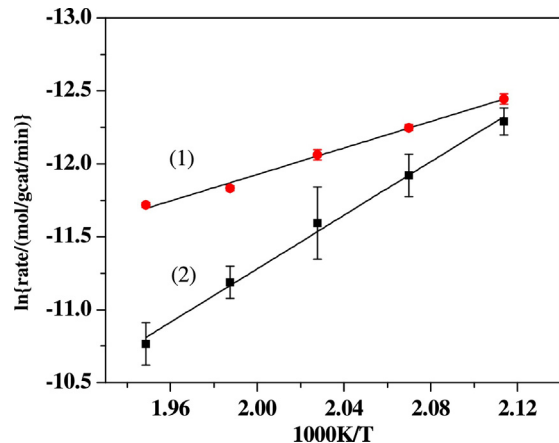


Fig. 10. Arrhenius plot for methanol production (1) and CO production (2) over CuCeTiO_x-CP.

and CuO/ZnO(0 0 0 1) surfaces were the most typical model surfaces in the kinetic study of methanol synthesis [55–61]. The current study provides a comparison of the CuCeTiO_x catalyst (30%CuO35%CeO₂35%TiO₂, prepared by co-precipitation) with these most studied model surfaces and supported catalysts.

The apparent activation energy of methanol production was estimated over the CuCeTiO_x catalyst by varying the reaction temperatures from 573 K to 613 K. The conversion was controlled below 7% in all the experiments to allow the assumption of a differential reactor. Fig. 10 shows the Arrhenius plot for methanol synthesis, giving an apparent activation energy of 9.1 ± 0.4 kcal/mol. This value is much lower than those for most commonly used Cu-based methanol synthesis catalysts, as compared in Table 5.

Surface science experiments showed that promoters and oxide supports have a significant influence on the activation energies for both methanol production and RWGS. On the Cu(1 1 1) surface, whether under ultrahigh vacuum (UHV) or high pressure of 0.5 MPa, the activation energy of methanol synthesis is about 25 kcal/mol [30,55]. The addition of ZnO decreases the activation energy from 25 to 16 kcal/mol [30,55]. The introduction of reducible oxide supports, such as ZrO₂ [62] and CeO₂ [30], also significantly decreases the activation energy. The activation energy of RWGS is slightly lower than methanol synthesis on all these model surfaces.

The experimental results of supported Cu catalysts evaluated under high pressure were quite different from surface science

studies. The activation barriers for methanol synthesis are generally about a factor of two lower than those of RWGS for all catalysts. Supported Cu catalysts such as Cu/ZnO and Cu/ZrO₂ also showed a lower activation energy of 8–11 kcal/mol and 10 kcal/mol, respectively. In comparison, supported Cu catalysts showed an activation energy for RWGS of 20–30 kcal/mol, which was much higher than the values from model surfaces.

In the current study, the activation energy for methanol synthesis over CuCeTiO_x is 9.1 ± 0.4 kcal/mol, which is lower than most catalysts listed in Table 5, and very close to that measured on the Cu/CeO_x/TiO₂(110) surface in UHV experiments. The activation energy for RWGS over CuCeTiO_x is 18.2 ± 0.7 kcal/mol, which is the lowest among the supported catalysts listed in Table 5. The lower activation energy for CO₂ conversion to either methanol or CO might be ascribed to the oxygen vacancies created in the solid solution of CeTiO_x, which facilitated the adsorption and activation of CO₂ over the catalysts.

4. Conclusions

Based on the results and discussion presented above, the following conclusions can be made regarding the enhanced catalytic properties of CuTiCeO_x for CO₂ hydrogenation to methanol:

- (1) The CuCeTiO_x catalyst showed a significant enhancement in activity, presenting 7 and 12 times higher CO₂ conversion than CuCeO_x and CuTiO_x, respectively. In addition, the CuCeTiO_x catalyst showed over 5 times higher surface area compared with the binary oxide catalysts.
- (2) The component concentrations of CuCeTiO_x had a significant influence on the catalytic performance, with a CeO₂/TiO₂ weight ratio of 1 being optimum. The increase in the CuO content slightly increased the CO₂ conversion.
- (3) The preparation method also had an effect on the surface composition of CuCeTiO_x and thus affected its catalytic performance.
- (4) The activation energy for methanol synthesis over CuCeTiO_x was much lower than other common Cu-based catalysts, confirming the significant synergistic effect in the ternary oxide catalysts.

Acknowledgements

The authors gratefully acknowledge the financial supports by the National Natural Science Foundation of China (Nos. 21673125 and 21276135). We acknowledge Ms. Lili Lin and Prof. Ding Ma of Peking University for their help in the CO₂ TPD experiments.

References

- [1] G.A. Olah, A. Goeppert, G.K.S. Prakash, *J. Org. Chem.* 74 (2009) 487–498.
- [2] M.D. Porosoff, B. Yan, J.G. Chen, *Energy Environ. Sci.* 9 (2016) 62–73.
- [3] M. Saito, *Catal. Surv. Jpn.* 2 (1998) 175–184.
- [4] S. Saeidi, N.A.S. Amin, M.R. Rahimpour, *J. CO₂ Util.* 5 (2014) 66–81.
- [5] X. Jiang, N. Koizumi, X. Guo, C. Song, *Appl. Catal., B* 170–171 (2015) 173–185.
- [6] S. Posada-Pérez, F. Viñes, J.A. Rodriguez, F. Illas, *Top. Catal.* 58 (2015) 159–173.
- [7] J.A. Rodriguez, P. Liu, D.J. Stacchiola, S.D. Senanayake, M.G. White, J.G. Chen, *ACS Catal.* 5 (2015) 6696–6706.
- [8] Y. Chen, S. Choi, L.T. Thompson, *ACS Catal.* 5 (2015) 1717–1725.
- [9] M.U. Khan, L. Wang, Z. Liu, Z. Gao, S. Wang, H. Li, W. Zhang, M. Wang, Z. Wang, C. Ma, J. Zeng, *Angew. Chem. Int. Ed.* 55 (2016) 1–6.
- [10] X. Yang, S. Kattel, S.D. Senanayake, J.A. Boscoboinik, X. Nie, J. Graciani, J.A. Rodriguez, P. Liu, D.J. Stacchiola, J.G. Chen, *J. Am. Chem. Soc.* 137 (2015) 10104–10107.
- [11] Y. Hartadi, D. Widmann, R.J. Behm, *ChemSusChem* 8 (2015) 456–465.
- [12] K. Samson, M. Śliwa, R.P. Socha, K. Góra-Marek, D. Mucha, D. Rutkowska-Zbić, J. Paul, M. Ruggiero-Mikolajczyk, R. Grabowski, J. Słoczyński, *ACS Catal.* 4 (2014) 3730–3741.
- [13] G.A. Olah, *Angew. Chem. Int. Ed.* 44 (2005) 2636–2639.
- [14] J.S. Lee, K.I. Moon, S.H. Lee, S.Y. Lee, Y.G. Kim, *Catal. Lett.* 34 (1995) 93–99.
- [15] T.S. Askgaard, J.K. Norskov, C.V. Ovesen, P. Stoltze, *J. Catal.* 156 (1995) 229–242.
- [16] L. Angelo, K. Kobl, L.M.M. Tejada, Y. Zimmermann, K. Parkhomenko, A. Roger, *C.R. Chim.* 18 (2015) 250–260.
- [17] G.X. Qi, X.M. Zheng, J.H. Fei, Z.Y. Hou, *Catal. Lett.* 72 (2001) 191–196.
- [18] J. Xiao, D. Mao, X. Guo, J. Yu, *Appl. Surf. Sci.* 338 (2015) 146–153.
- [19] J.B. Wang, H.K. Lee, T.J. Huang, *Catal. Lett.* 83 (2002) 79–86.
- [20] F. Arena, G. Mezzatesta, G. Zafarana, G. Trunfio, F. Frusteri, L. Spadaro, *Catal. Today* 210 (2013) 39–46.
- [21] F. Arena, G. Mezzatesta, G. Zafarana, G. Trunfio, F. Frusteri, L. Spadaro, *J. Catal.* 300 (2013) 141–151.
- [22] P. Gao, F. Li, N. Zhao, F. Xiao, W. Wei, L. Zhong, Y. Sun, *Appl. Catal. A* 468 (2013) 442–452.
- [23] V.A. Matyshak, O.N. Sil'Chenkova, I.T. Ismailov, V.F. Tret'Yakov, *Kinet. Catal.* 53 (2012) 91–100.
- [24] C. Li, X. Yuan, K. Fujimoto, *Appl. Catal. A* 469 (2014) 306–311.
- [25] J. Toyir, P.R.R. de la Piscina, J.L.G. Fierro, N.S. Homs, *Appl. Catal. B* 29 (2001) 207–215.
- [26] M. Saito, T. Fujitani, M. Takeuchi, T. Watanabe, *Appl. Catal. A* 138 (1996) 311–318.
- [27] C.G. Maciel, T.D.F. Silva, E.M. Assaf, J.M. Assaf, *Appl. Energy* 112 (2013) 52–59.
- [28] J.B. Park, J. Graciani, J. Evans, D. Stacchiola, S.D. Senanayake, L. Barrio, P. Liu, J.F. Sanz, J. Hrbek, J.A. Rodriguez, *J. Am. Chem. Soc.* 132 (2010) 356–363.
- [29] J.B. Park, J. Graciani, J. Evans, D. Stacchiola, S. Ma, P. Liu, A. Nambu, J.F. Sanz, J. Hrbek, J.A. Rodriguez, *Proc. Natl. Acad. Sci. U. S. A.* 106 (2009) 4975–4980.
- [30] J. Graciani, K. Mudiyanselage, F. Xu, A.E. Baber, J. Evans, S.D. Senanayake, D.J. Stacchiola, P. Liu, J. Hrbek, S.J. Fernandez, J.A. Rodriguez, *Science* 345 (2014) 546–550.
- [31] M. Behrens, D. Brennecke, F. Girsdsies, S. Kißner, A. Trunschke, N. Nasrudin, S. Zakaria, N.F. Idris, S.B.A. Hamid, B. Kniep, R. Fischer, W. Busser, M. Muhler, R. Schlögl, *Appl. Catal., A* 392 (2011) 93–102.
- [32] M. Behrens, R. Schlögl, Z. Anorg. Allg. Chem. 639 (2013) 2683–2695.
- [33] Y. Zhu, X. Kong, X. Zhu, F. Dong, H. Zheng, Y. Zhu, Y. Li, *Appl. Catal., B* 166 (2015) 551–559.
- [34] X. Gao, X. Du, L. Cui, Y. Fu, Z. Luo, K. Cen, *Catal. Commun.* 12 (2010) 255–258.
- [35] J. Huang, Y. Kang, T. Yang, Y. Wang, S. Wang, *React. Kinet. Mech. Catal.* 104 (2011) 149–161.
- [36] S. Watanabe, X. Ma, C. Song, *J. Phys. Chem. C* 113 (2009) 14249–14257.
- [37] W. Shan, F. Liu, H. He, X. Shi, C. Zhang, *Catal. Today* 184 (2012) 160–165.
- [38] P. Li, Y. Xin, Q. Li, Z. Wang, Z. Zhang, L. Zheng, *Environ. Sci. Technol.* 46 (2012) 9600–9605.
- [39] E. Sheerin, G.K. Reddy, P. Smirniotis, *Catal. Today* 263 (2016) 75–83.
- [40] H.Y. Xiao, W.J. Weber, *J. Phys. Chem. B* 115 (2011) 6524–6533.
- [41] K.B. Sravan Kumar, P.A. Deshpande, *J. Phys. Chem. C* 119 (2015) 8692–8702.
- [42] O.H. Laguna, A. Pérez, M.A. Centeno, J.A. Odriozola, *Appl. Catal., B* 176–177 (2015) 385–395.
- [43] C. Yoo, D. Lee, M. Kim, D.J. Moon, K. Lee, *J. Mol. Catal. A: Chem.* 378 (2013) 255–262.
- [44] K. Samson, M. Śliwa, R.P. Socha, K. Góra-Marek, D. Mucha, D. Rutkowska-Zbić, J. Paul, M. Ruggiero-Mikolajczyk, R. Grabowski, J. Słoczyński, *ACS Catal.* 4 (2014) 3730–3741.
- [45] A. Bansode, B. Tidona, P. Rohr, A. Urakawa, *Catal. Sci. Technol.* (2013).
- [46] Z. Wang, Z. Xu, S. Peng, M. Zhang, G. Lu, Q. Chen, Y. Chen, G. Guo, *ACS Catal.* 5 (2015) 4255–4259.
- [47] M. Saito, T. Fujitani, I. Takahara, T. Waranabe, M. Takeuchi, Y. Kanai, K. Moriya, T. Kakumoto, *Energy Convers. Manag.* 36 (1995) 577–580.
- [48] K.K. Bando, K. Sayama, H. Kusama, *Appl. Catal. A* 165 (1997) 391–409.
- [49] N. Nomura, T. Tagawa, S. Goto, *Appl. Catal., A* 166 (1998) 321–326.
- [50] L. Chen, Z. Si, X. Wu, D. Weng, *ACS Appl. Mater. Interfaces* 6 (2014) 8134–8145.
- [51] B. Yang, Y. Shen, Y. Zeng, S. Shen, S. Zhu, *J. Rare Earth* 34 (2016) 268–275.
- [52] L. Matějová, K. Kočí, M. Reli, L. Čapek, A. Hospodková, P. Peikertová, Z. Matěj, L. Obalová, A. Wach, P. Kuštrawski, A. Kotarba, *Appl. Catal., B* 152–153 (2014) 172–183.
- [53] M. Burgos, M. Langlet, J. Sol-Gel Sci. Technol. 16 (1999) 267–276.
- [54] S. Kattel, B. Yan, Y. Yang, J.G. Chen, P. Liu, *J. Am. Chem. Soc.* 138 (2016) 12440–121245.
- [55] Y. Yang, J. Evans, J.A. Rodriguez, M.G. White, P. Liu, *Phys. Chem. Chem. Phys.* 12 (2010) 9909.
- [56] Y. Zhao, Y. Yang, C. Mims, C.H.F. Peden, J. Li, D. Mei, *J. Catal.* 281 (2011) 199–211.
- [57] L. Martínez-Sáez, N. Siemer, J. Frenzel, D. Marx, *ACS Catal.* 5 (2015) 4201–4218.
- [58] Y. Yang, M.G. White, P. Liu, *J. Phys. Chem. C* 116 (2012) 248–256.
- [59] Y. Kim, T.S.B. Trung, S. Yang, S. Kim, H. Lee, *ACS Catal.* 6 (2016) 1037–1044.
- [60] S.D. Senanayake, P.J. Ramírez, I. Waluyo, S. Kundu, K. Mudiyanselage, Z. Liu, Z. Liu, S. Axnanda, D.J. Stacchiola, J. Evans, J.A. Rodriguez, *J. Phys. Chem. C* 120 (2016) 1778–1784.
- [61] M.J. Lyle, O. Warschkow, B. Delley, C. Stampfl, *Surf. Sci.* 641 (2015) 97–104.
- [62] X. Guo, D. Mao, G. Lu, S. Wang, G. Wu, *J. Mol. Catal. A: Chem.* 345 (2011) 60–68.
- [63] A. Karelovic, *Catal. Sci. Technol.* 5 (2014) 869–881.
- [64] X. Guo, D. Mao, G. Lu, S. Wang, G. Wu, *J. Catal.* 271 (2010) 178–185.